Journal of Catalysis 287 (2012) 76–85

Contents lists available at SciVerse ScienceDirect

Journal of Catalysis

journal homepage: www.elsevier.com/locate/jcat

Efficient Sc triflate mesoporous-based catalysts for the synthesis of 4,4′-methylenedianiline from aniline and 4-aminobenzylalcohol

Natalia Candu [a], Madalina Ciobanu [a], Petru Filip [b], Jamal El Haskouri [c,d], Carmen Guillem [c], Pedro Amoros [c,*], Daniel Beltran [c], Simona M. Coman [a,*], Vasile I. Parvulescu [a,*]

[a] University of Bucharest, Department of Organic Chemistry and Catalysis, Bdul Regina Elisabeta 4-12, 030016 Bucharest, Romania
[b] "Costin D. Neniţescu" Institute of Organic Chemistry of the Romanian Academy, Spl. Independentei 202B, 71141 Bucharest, Romania
[c] Institut de Ciència dels Materials, Universitat de València, P.O. Box 22085, 46071 Valencia, Spain
[d] Fundació General, Universitat de València, P.O. Box 22085, 46071 Valencia, Spain

ARTICLE INFO

Article history:
Received 25 July 2011
Revised 13 November 2011
Accepted 2 December 2011
Available online 2 January 2012

Keywords:
4-Aminobenzylalcohol
Aniline
4,4′-Methylenedianiline
Scandium triflate
Bimodal mesoporous materials
Atrane method
Microwaves

ABSTRACT

Sc triflate mesoporous-based catalysts have been prepared using a two-step strategy (i.e., Atrane method) based on the formation of the hierarchic bimodal porosity in the first step and the formation of Sc triflate complexes at the materials surface in the second step. All solids were analyzed by EPMA, surface area, and pore size values, XRD, TEM, FTIR, and ^{45}Sc NMR static spectra. The catalysts have been investigated in the synthesis of 4,4′-methylenedianiline (4,4′-MDA) from aniline and 4-aminobenzylalcohol. 4,4′-MDA was obtained with selectivities over 85.0% for a conversion of aniline of 31%, at 80 °C and after 24 h. Using microwaves, selectivities of 90% in 4,4′-MDA were reached in only 3 h. Important key parameters influencing the catalytic performances seem to be the scandium content and the nature of the formed Sc species. By replacing formaldehyde with 4-aminobenzylalcohol, the necessity of additional steps for neutralization and separation of the wastes can be eliminated.

1. Introduction

Methylenedianiline (MDA) is a key intermediate for the production of polyurethanes with an annual production higher than two million metric tonnes. Unfortunately, the industrial production is still performed by reacting formaldehyde with stoichiometric amounts of HCl and aniline requiring additional steps for neutralization and separation and also producing large amount of residual salt water that needs to be treated before disposal [1]. A cleaner alternative to this synthesis by using solid catalysts is therefore highly desirable.

On the other hand, the use of formaldehyde and aniline as raw materials together with diamines led to higher molecular weight species (triamines, tetraamines, etc.). However, the formation of the 4,4′-MDA product can be carefully managed by controlling the aniline: formaldehyde ratio, the catalyst content, and reaction temperature. Thus high aniline: formaldehyde ratio and low temperatures generally favor its formation. Unfortunately, the use of exceeds of one of reactants (i.e., aniline, in this case) generates additional wastes. Moreover, *N*-methylated products and quinazolines can also be formed under these conditions leading to a decrease of the yields.

Although there are numerous papers reporting the improvement of the synthesis by replacing the HCl with solid catalysts as ion exchange resins [2], clays [3], Y-, β-, ZSM-5, and fluorine-treated dealuminized Y-type zeolites [4–8], an additional improvement may be done by replacing the formaldehyde with 4-aminobenzylalcohol reactant. In this way, the synthesis of 4,4′-MDA may be substantially improved in terms of productivity and simplicity thus avoiding the formation of by-products and eliminating the necessity of additional steps for neutralization and separation of the reaction products.

In heterogeneous acidic catalysis, isolated species usually are much more active than oligomeric and polymeric species. In conventional co-hydrolysis methods, good dispersion of monomeric metallic species in the silica network is not easily achieved. A fluoride catalyzed route for the synthesis of catalytically active non-ordered mesoporous silica-based materials in the absence of surfactants was developed by Rey and co-workers [9]. The synthesis procedure has allowed the introduction of different organic and inorganic functionalities with specific chemical activities within silica networks with well-tailored mesoporous distributions. Particularly,

* Corresponding authors. Fax: +40 214100241 (V.I. Parvulescu).
E-mail addresses: v_parvulescu@yahoo.com, vasile.parvulescu@g.unibuc.ro (V.I. Parvulescu).

0021-9517/$ - see front matter © 2011 Elsevier Inc. All rights reserved.
doi:10.1016/j.jcat.2011.12.008

this sol–gel synthesis route has permitted the synthesis of Al- and Ti-containing mesoporous silica materials that have been found to be catalytically active for acid and redox processes, respectively. Recently, we reported that Atrane route to synthesis of Sn-MCM-41 [10] and Al-UVM-7 (UVM = University of Valencia Materials) [11] is an effective solution for the preparation of well dispersed acid Sn and Al triflate species into the framework of the mesoporous silica. The obtained materials were active and highly selective into a number of important fine chemicals synthesis as the acylation of aromatic sulfonamides, the synthesis of (*dl*)-[α]-tocopherol, or the synthesis of non-ionic surfactants structures [10,12]. In spite of the well-known similarity between Sc(III) and Al(III) (given by its small ionic radius (0.73 Å) and identical charge (III)), reports dealing with the replacement of Si for Sc are extremely limited. In fact, as far as we known, only one recently report describing the incorporation of Sc sites in ZSM-5 zeolite network was published [13]. In a similar way, no examples of Sc inclusion in the framework of mesoporous silica materials exist and only some examples of incorporation through impregnation with complex solutions or grafting being described [14]. On the other hand, according to the studies of Kobayashi et al. [15], scandium triflate is a water-compatible strong Lewis acid with a large applicability in organic synthesis.

Taking into account this information and with the aim to create robust catalysts with strong Lewis acidity for the 4,4′-MDA synthesis from aniline and 4-aminobenzylalcohol, we prepared a series of ScOTf-UVM-7 mesoporous bimodal catalysts. The Atrane method allows the Sc incorporation inside the UVM-7 silica walls in a first step, then, through heating the Sc-containing mesoporous silicas in solutions of triflic acid, the formation of Sc triflate complexes at the materials surface is performed.

2. Experimental

2.1. Catalyst preparation

All reagents were used as received from Sigma–Aldrich (tetraethyl orthosilicate (98%) [TEOS], scandium oxide (99.9%) [Sc_2O_3], triethanolamine (99%) [$N(CH_2–CH_2–OH)_3$, hereinafter TEA], cetyltrimethylammonium bromide (99%) [CTABr], triflic acid (98%), and methanol (99.8%)).

ScOTf-UVM-7 porous bimodal catalysts were prepared in a two-step strategy (i.e., Atrane method) based on the use of complexes that include TEA-related ligand species (named Atrane ligands) as hydrolytic inorganic precursors. The formation of the hierarchic bimodal porosity occurs during the first step. The pH provided by the triethanolamine–water medium (pH ≈ 9) favors the nucleation and growth of mesoporous nanoparticles and the subsequent aggregation leads to a controlled textural-like meso/macroporosity [16–18]. The resulted solids have been denoted as Sc-UVM(x) (x = Sc/Si molar ratio × 10^3). The second step corresponds to the heating the Sc-containing mesoporous silicas in solutions of triflic acid with the formation of Sc triflate complexes at the materials surface. The obtained catalysts were designated ScOTf-UVM(x) (x = the final Sc/Si atomic ratio after reaction with triflic acid × 10^3).

Details of a typical synthesis leading to Sc-UVM(50) sample can be described as follows: a mixture (suspension) of Sc_2O_3 (0.11 g, 8.23×10^{-4} mol) and TEOS (11 mL, 0.05 mol) was slowly added to liquid TEA (23 mL, 0.173 mol). This mixture was heated at 150 °C for 10 min (with stirring) leading to a solution containing Sc and Si-atrane complexes. After cooling of the previous solution to 90 °C, CTABr (4.689 g, 0.013 mol) was added under continuous stirring to favor the surfactant dissolution. This solution was forward cooled to 60 °C and mixed with water (80 mL, 4.44 mol). After a few seconds, a white powder appeared and was allowed to age at room temperature for 4 h. The final mesostructured powder was filtered off, washed with water and ethanol, and air-dried. In order to open the pore system, the as-synthesized solid was heated at 550 °C (1 °C/min) under static air atmosphere for 7 h. In all cases, the molar ratio of the reagents in the mother liquor was adjusted to $(2-\delta)$ Si/δ Sc/7 TEA/0.52 CTABr/180 H_2O (where $n = \delta/(2-\delta)$ = 0.007, 0.010, 0.016, 0.025, and 0.1).

The second step corresponds to the formation of Sc triflate complexes at the Sc-UVM-7 surface. In a typical synthesis leading to ScOTf-UVM(50) sample, 1 g of Sc-UVM(50) was suspended in a mixture of triflic acid (5 g) and methanol (35 ml). This mixture was stirred under reflux for 4 h at *ca.* 70 °C. The resulting porous samples were collected by filtration, washed with methanol to eliminate any excess triflic acid, and air-dried.

2.2. Catalyst characterization

All solids were analyzed for Si, Sc, and S by electron probe microanalysis (EPMA) using a Philips SEM-515 instrument. Si/Sc and S/Sc molar ratio values averaged from EPMA data are summarized in Table 1. X-ray powder diffraction (XRD) data were recorded on a Seifert 3000TT θ–θ diffractometer using Cu Kα radiation. Low-angle patterns were collected in steps of 0.02° (2θ) over the angular range 1–10° (2θ) for 25 s per step. In order to detect the presence of some crystalline bulk phase, additional patterns were collected with a bigger scanning step [0.05°(2θ)) over a wide angular range (10–70°(2θ)] and a lower acquisition time (10 s. per step). The Sc_2O_3 particle size was estimated using the Scherrer equation assuming spherical particles. For this purpose, XRD patterns with a good statistic (scanning step of 0.02°(2θ) and 20 s. per step) were recorded over specific angular ranges around the (222), (440), and (622) reflections of the Sc_2O_3 cubic phase (JCPDS 43-1028). Transmission electron microscopy (TEM) images were acquired with a JEOL JEM-1010 instrument operating at 100 kV. Surface area and pore size values were calculated from nitrogen adsorption–desorption isotherms (−196 °C) recorded on a Micromeritics ASAP-2010 instrument. Calcined samples were degassed for 15 h at 130 °C and 10^{-6} Torr before analysis. Surface areas were estimated according to the BET model, and pore size dimensions were calculated using the BJH method. FTIR spectra were collected on a Nicolet 4700 spectrometer (200 scans with a resolution of 4 cm^{-1}) using self disks of 1% sample in KBr. NH_3-DRIFT spectra were collected with the same type of spectrometer using the following program: treatment of the catalysts under a He flow (30 mL min^{-1}) for 1 h at room temperature and then for another hour at 150 °C after heating the catalysts with a slope rate of 5 °C min^{-1}. After cooling at room temperature, a flow of NH_3 (10% in He) of 30 mL min^{-1} was flushed for 30 min. Then, a He flow (30 mL min^{-1}) was flushed for 30 min and the first spectrum was recorded. Other spectra were collected after heating the samples in He till 150 °C with a slope rate of 5 °C min^{-1}. Spectra were collected at 50, 100, and 150 °C, respectively. ^{45}Sc NMR static spectra were recorded on a Varian Unity 300 spectrometer at 97.15 MHz. The chemical shifts were referenced to $ScCl_3$ aqueous solution at 0 ppm.

2.3. Catalytic tests

Activity tests in batch mode were carried out as described in the following procedure: aniline (1–2 mmol, 93–186 mg) was mixed with 4-aminobenzylalcohol (1 mmol, 123 mg) in 3 ml of solvent (acetonitrile, THF, hexane, or ethanol) into a vial glass of 20 mL capacity. To this mixture, the catalyst (10–30 mg) was added and heated up to 80 °C, under stirring (1.400 rpm), for 2–24 h. For comparison, tests with homogeneous Sc triflate (99%, Aldrich) and SAC-13 (13 wt.% Nafion/silica: 0.15 meq H^+/g; S_{sp} (m^2/g) = 400; D_p

Table 1
Selected synthetic and physical data for Sc-UVM-7 and ScTf-UVM-7 porous materials.

Sample	Sc/Si[a]/n	Sc/Si[b]/x	S/Si[b]/y	S/Sc[b]/z	d_{100}[c]/nm	S_{BET}/m^2 g^{-1}	Small pore[d]/nm	Large pore[d]/nm	Small vol.[d]/cm^3 g^{-1}	Large vol.[d]/cm^3 g^{-1}	Pore wall[e]/nm
Sc-UVM(9)	0.007	0.009	–	–	4.01	1081.2	2.85	32.5	0.91	1.44	1.78
Sc-UVM(14)	0.010	0.014	–	–	3.92	1069.6	2.82	33.0	0.89	1.11	1.71
Sc-UVM(50)	0.016	0.050	–	–	3.87	1033.0	2.76	34.0	0.86	1.08	1.71
Sc-UVM(77)	0.025	0.077	–	–	3.85	1018.5	2.73	35.4	0.85	1.20	1.72
Sc-UVM(250)	0.100	0.250	–	–	3.84	728.0	2.65	44.7	0.56	1.04	1.78
ScOTf-UVM(9)	0.009	0.006	0.005	0.90	3.82	1160.0	2.70	52.4	0.92	1.38	1.71
ScOTf-UVM(14)	0.014	0.012	0.010	0.84	3.88	986.0	2.68	44.3	0.83	1.18	1.80
ScOTf-UVM(50)	0.050	0.037	0.015	0.40	3.85	990.8	2.63	30.7	0.8	1.22	1.81
ScOTf-UVM(77)	0.077	0.055	0.020	0.40	3.84	984.0	2.62	26.1	0.78	1.16	1.81
ScOTf-UVM(250)	0.250	0.166	0.038	0.23	3.75	680.0	2.60	34.1	0.53	0.95	1.73

[a] Sc/Si molar ratio in the mother liquor in the first preparative step (entries 1–5), or in the solids used in the second step (entries 6–10).
[b] Sc/Si, S/Si and S/Sc molar ratio values from EPMA.
[c] d-spacing values from XRD data.
[d] Mesopore diameters and total pore volume values calculated by using the BJH model on the adsorption branch of the isotherms (Small and large pore volumes has been determined from data at $P/P_0 < 0.6$ and $P/P_0 > 0.6$, respectively).
[e] Pore wall defined as $a_0 - \phi_{BJH}$.

(Å) = 100) were also preformed using the same reaction conditions. After reaction, the catalyst was filtered out and the reaction mixture analyzed by FID-GC, MS-GC chromatography, and ^1H and ^{13}C NMR spectroscopy (Bruker AV 400 spectrometer in $CDCl_3$ solvent. Chemical shift is expressed in δ (ppm) regarding to the tetramethylsilane (Me_4Si) used as internal standard). The activity of the catalysts was expressed as TON. TON was determined as the number of aniline molecules converted to the scandium triflates sites while the concentration of the Sc triflate was determined from the EPMA measurements.

3. Results and discussion

3.1. Catalyst characterization

At pH > 2.5 the Sc hydrolysis is much faster than the Si hydrolysis [19–21], the formation of $Sc(OH)_3$ being expected after water addition. Under the pH working conditions (pH ~ 9), in addition to this phase, several monomeric ($Sc(OH)_2^+$, $Sc(OH)_4^-$) and oligomeric ($Sc_3(OH)_5^{4+}$) species exist in equilibrium [19–21]. A solution to overcome or minimize the problems associated with the high reactivity differences of Si and Sc precursor species is to use the Atrane method synthesis. In this approach, triethanolamine (TEA) is used as a complexion agent able to keep the elements in homogeneous solution without extensive phase segregation even after water addition. While the formation of Si-TEA (silatrane) complexes is well documented [22], there are not references on the formation of Sc-TEA complexes, although atranes of chemically related trivalent elements such as Al, Ga, and Y have been previously described [23,24]. In any case, regardless the formation or not of atranes, the TEA concentrated solutions are able to induce a homogeneous formation of mixed or complex oxides, and this capability was used by ceramists to prepare heterometallic homogeneous oxides [25].

Therefore, the formation of Sc-UVM-7 mesophases must be viewed as a consequence of the coexistence of two chemical processes: (1) the nucleation and growth of $Sc(OH)_3$ particles in equilibrium with several monomers and small olygomers (this process probably starts previously to the silica network formation due to the high insolubility of the Sc species under the working conditions used), and (2) the formation of the silica mesophase, which should act as a chemically inert supramolecular fixative agent able to capture both $Sc(OH)_3$ particles and also Sc-containing solution species previously formed. The relatively fast silica mesophase formation when CTA^+ surfactant is used (due to the strong ionic S^+I^- bonds involved) should favor a good dispersion of $Sc(OH)_3$ particles and isolated Sc sites along the pore walls. Finally, the thermal treatment of the as-synthesized solids leads to the pore opening and the formation of Sc_2O_3.

Data from Table 1 confirm the fast hydrolysis rate of Sc species and the high insolubility of the $Sc(OH)_3$ when compared to the silica counterpart. In fact, the real scandium content (x) is clearly higher than the nominal one (n), and this tendency increases with the scandium content (from Sc-UVM(9) to Sc-UVM(250) sample). The Sc is practically removed of the solution in a complete way by formation of oxidic nanodomains, while a certain proportion of Si-based olygomers in equilibrium with the solid remains as soluble species.

The preservation of the UVM-7-like mesostructured is confirmed by XRD and TEM. All Sc-UVM-7 samples display diffraction patterns in the low-angle domain (Fig. 1) with one strong reflection and a broad signal of relatively low intensity. Although these patterns cannot be associated with a highly ordered 2-D hexagonal array as occurs for MCM-41 materials, a certain order degree seems to be preserved. This partial order lost is due to the relatively low pH conditions used when compared to the MCM-41 phases, and also to the effect of the heteroelement (Sc) incorporation. Then, in a roughly way, the intense signal and the shoulder can be indexed to the (100) and the overlapped (110) and (200) reflections, respectively (assuming a pseudo-hexagonal array). A smooth evolution of the $d_{(100)}$ distance is observed as the Sc content increases, suggesting that the heteroelement is progressively incorporated inside the mesostructure. Moreover, the high-angle XRD patterns (Fig. 2) confirm the existence of crystalline Sc_2O_3. The proportion of this phase also increases with the Sc content. At this point, the success of the Atrane method is supported by TEM images that allow discarding segregation of large Sc_2O_3 particles. Images of medium magnification confirm the absence of non-porous particles that could be ascribed to scandium oxide. In fact, in the case of Sc-UVM(14) – Sc-UVM(77) samples, TEM images (Fig. 3) are practically indistinguishable from those of pure UVM-7 silica and confirm that two pore systems are present: intraparticle mesopores (white spots in the TEM images in Fig. 3) and large inter-particle pores of textural-like. On the other hand, the above-mentioned absence of large-scale Sc_2O_3 segregation suggests that the Sc_2O_3 particles must be present in the form of small nanodomains partially embedded inside the silica-based pore walls. Then, although a small segregation in the form of micrometric Sc_2O_3 particles cannot be completely discarded, magnified TEM images (inset of Fig. 3b) are consistent with a homogeneous nano-dispersion of Sc_2O_3 domains (black spots) forming in a cooperative way with the amorphous silica the mesopore walls.

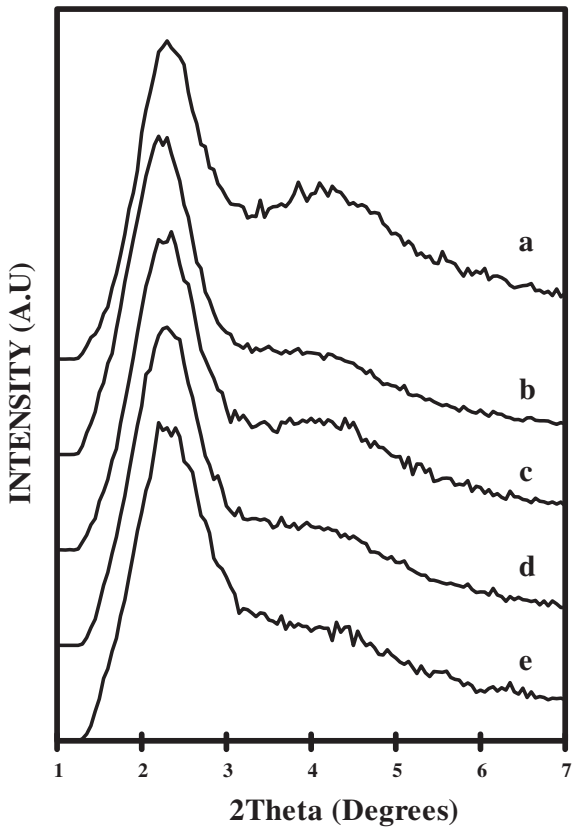

Fig. 1. Low-angle XRD patterns of (a) Sc-UVM(9), (b) Sc-UVM(14), (c) Sc-UVM(50), (d) Sc-UVM(77), and (e) Sc-UVM(250).

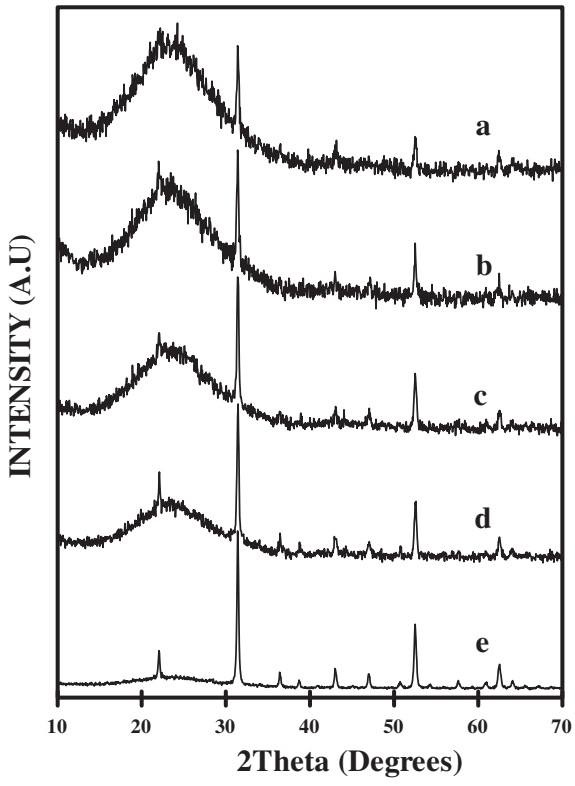

Fig. 2. High-angle XRD patterns of (a) Sc-UVM(9), (b) Sc-UVM(14), (c) Sc-UVM(50), (d) Sc-UVM(77), and (e) Sc-UVM(250).

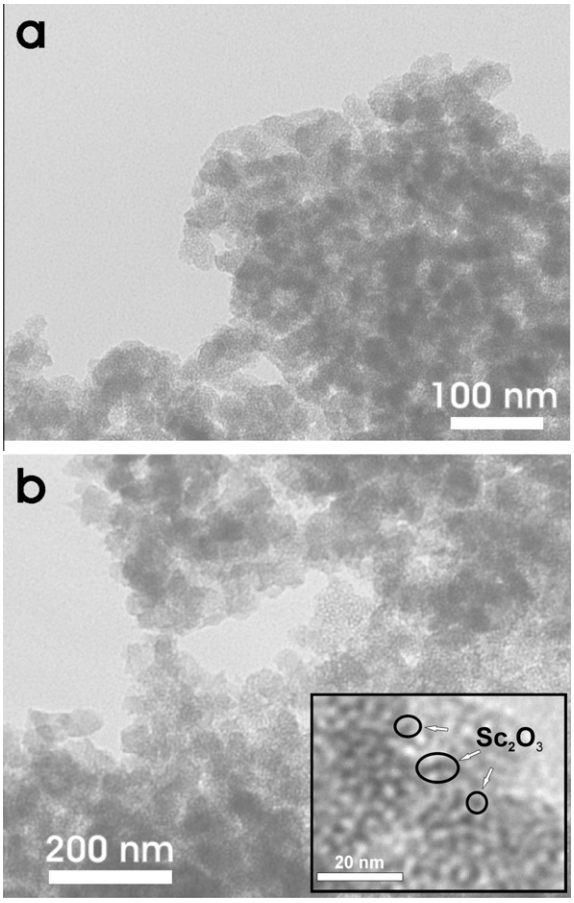

Fig. 3. Representative TEM image of the Sc-UVM-7 materials. (a) Sc-UVM(14), and (b) Sc-UVM(77). The enlarged image in the inset shows dark spots ascribed to scandium oxide nanodomains.

These black spots are dimensions ranging from 4 to 10 nm. The small domains (around 4 nm) show spherical or pseudo-spherical shapes, and the largest ones display irregular shapes, probably due in some cases to a certain aggregation of small spherical nanoparticles.

The existence of a bimodal hierarchic pore organization is further confirmed through N_2 adsorption–desorption isotherms (Fig. 4). The curves show, in all cases, a well-defined adsorption step at intermediate relative pressure ($0.2 < P/P_0 < 0.4$ range) corresponding to the filling of the intra-particle mesopores. The second

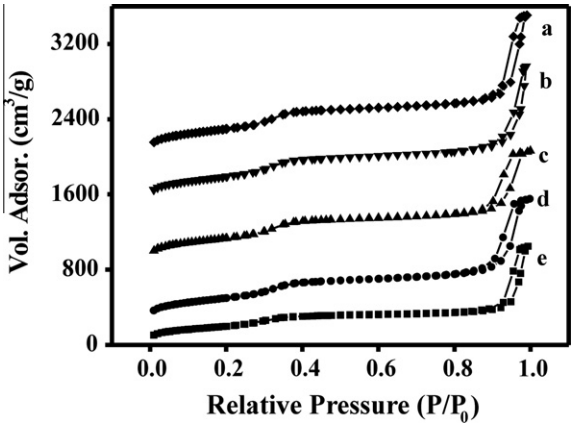

Fig. 4. N_2 adsorption–desorption isotherms of (a) Sc-UVM(9), (b) Sc-UVM(14), (c) Sc-UVM(50), (d) Sc-UVM(77), and (e) Sc-UVM(250).

adsorption step, at a high relative pressure, can be associated with the filling of the inter-particle large textural pores. As the Sc content increases, surface area, intra-particle mesopore size, and pore volume decrease in a progressive way (see Table 1).

The evolution is practically negligible in the $0.009 < x < 0.077$ range, and the slightly more accused BET area and pore volume decrease in Sc-UVM(250) sample ($x = 0.25$) could be due to the existence of a low proportion of large Sc_2O_3 crystals in the final sample (according to XRD). The intra-particle large pore (in the domain of large mesopores) also remains practically unchanged from Sc-UVM(9) to Sc-UVM(77) samples, and a slight size increase is observed for Sc-UVM(250) sample. From combination of XRD and adsorption data, the thickness of the intra-particle mesopore walls (defined as a_0 – BJH pore size) is practically constant regardless the Sc content.

During the second synthesis step, the accessible Sc sites at the pore wall surface of the Sc-UVM-7 solids interact with triflic acid to form the corresponding triflate complexes. EPMA analysis shows that all samples are chemically homogeneous with a regular distribution of Si, Sc, and S atoms throughout the inorganic walls at the micrometer level (spot area ≈1 μm). Hence, the solids can be considered as monophasic products at micrometric scale.

The inclusion of triflate species inside the Sc-UVM-7 is confirmed by EPMA: the S/Si molar ratio increases in a gradual way with the Sc content (from 0.005 to 0.038). On the other hand, when a Sc-free UVM-7 sample was processed with triflic acid exactly under the same conditions, no incorporation of triflate ligands occurs according to elemental analysis and EPMA. These data suggest that, as expected, the triflate ligands must be preferentially located on the Sc atoms. Simultaneously, it can be observed that a significant loss of Sc occurs. The Sc/Si molar ratio in the ScOTf-UVM-7 samples is lower than in the corresponding Sc-UVM-7 solids, and this effect increase with the Sc content. Moreover, a gradual decrease in the S/Sc molar ratio is observed from ScOTf-UVM(9) to ScOTf-UVM(250) samples.

These trends could be due to several competitive processes: (1) the progressive formation of Sc_2O_3 nanodomains as the Sc content increases, (2) the solubility of the accessible Sc_2O_3 particles in triflic acid media (probably due to the formation of the Sc triflate complexes and the subsequent leaching through washing, and according to XRD (see below)), and (3) the inefficacy of this nanodomains to coordinate with triflic acid ligands when compared to isolated Sc sites (see below). Moreover, it is necessary to consider that only a certain proportion of Sc sites are located at the surface and the remaining Sc atoms, inside the pore walls, cannot be accessible to the triflate ligands. Based on these considerations, it can be assumed that the number of triflate ligands around the active Sc sites must be larger than the S/Sc molar ratio values presented in Table 1.

The treatment with triflic acid does not alter the UVM-7-like architecture at mesoscopic level. In fact, no appreciable differences between the low-angle XRD patterns of Sc-UVM-7 and ScOTf-UVM-7 samples (Fig. 5) can be appreciated. Both the intense (100) signal and the shoulder are preserved for all samples. The detection of this last unresolved broad signal is typical of hexagonal disordered mesopore arrays. Once established the absence of mesostructure degradation after the two preparative steps, it must be noted that the triflic acid treatment alters in a different way the possible Sc species included in the pore walls. Therefore, high -angle XRD patterns (Fig. 6) show that after the treatment with triflic acid, a significant decrease in the intensity of the diffraction peaks of Sc_2O_3 occurs, and this effect is more pronounced for samples having low Sc contents. Based on the evolution of the XRD patterns, it can be established three regimes: (1) in the case of catalysts with lower Sc content (ScOTf-UVM(9) and ScOTf-UVM(14) samples), the triflic acid practically leads to the complete

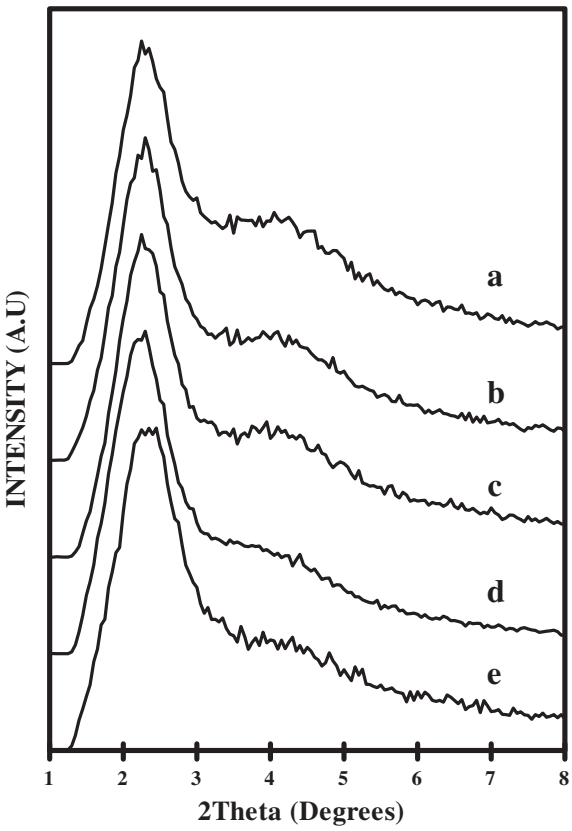

Fig. 5. Low-angle XRD patterns of (a) ScOTf-UVM(9), (b) ScOTf-UVM(14), (c) ScOTf-UVM(50), (d) ScOTf-UVM(77), and (e) ScOTf-UVM(250).

evolution of the Sc_2O_3 domains (only very small peaks are preserved) and consequently the dominant Sc sites must correspond to isolated or small olygomers in the form of triflate complexes at the pore surface, (2) for samples with medium Sc content (ScOTf-UVM(50) and ScOTf-UVM(77) samples), where only a partial evolution of the Sc_2O_3 domains occurs, a mixture of oxidic domains and Sc triflate complexes is expected, and (3) in the case of the richest Sc catalyst (ScOTf-UVM(250)), in spite of the appreciable intensity decrease of peaks attributed to Sc_2O_3, these nanodomains seem to be the more abundant Sc species. On the other hand, X-ray line broadening analysis using the Scherrer equation leads to average crystallite sizes of 4–6 nm and 8–9 nm for catalysts having low/medium and high Sc content, respectively.

TEM photographs show that the organization based on aggregates of mesoporous nanoparticles is maintained (Fig. 7). The intraparticle mesoporous can be clearly appreciated in the insets of Fig. 7b. Although regular hexagonal mesopore arrays can be observed in some particles, the disordered mesostructure is the dominant intraparticle organization. On the other hand, a significant decrease both in the intensity and density of black spots (Sc_2O_3 domains) is observed for all samples when comparing with samples before triflic acid treatment. This evolution is in accordance to XRD data.

The N_2 adsorption–desorption isotherms (Fig. 8) are in good accordance with TEM observations dealing with the existence of hierarchical porosity. All samples display isotherms with two well-defined adsorption steps at medium and high relative pressure values associated with the filling of the intra-particle mesopores and the textural pores, respectively.

High BET surface area values around 1000 m^2/g are preserved for ScOTf-UVM(9) to ScOTf-UVM(250) samples, and only a certain area decrease is observed for the richest Sc sample. No significant

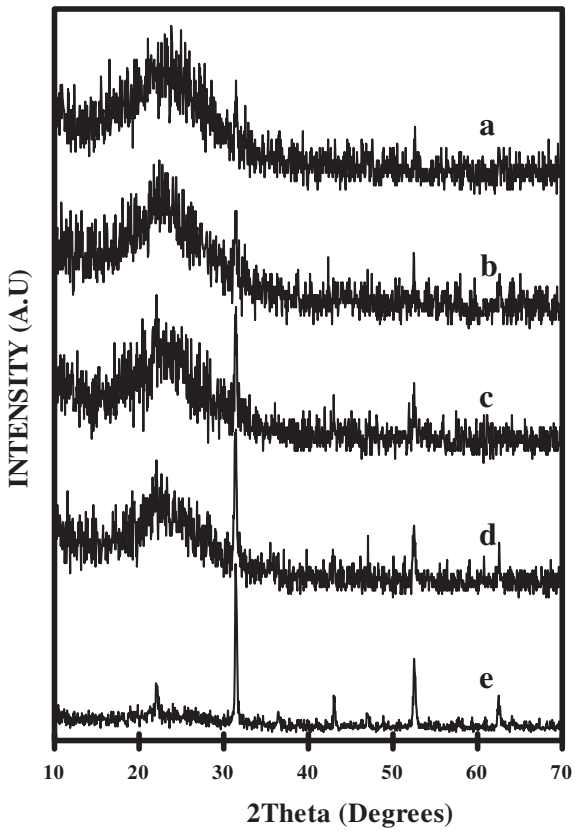

Fig. 6. High-angle XRD patterns of (a) ScOTf-UVM(9), (b) ScOTf-UVM(14), (c) ScOTf-UVM(50), (d) ScOTf-UVM(77), and (e) ScOTf-UVM(250).

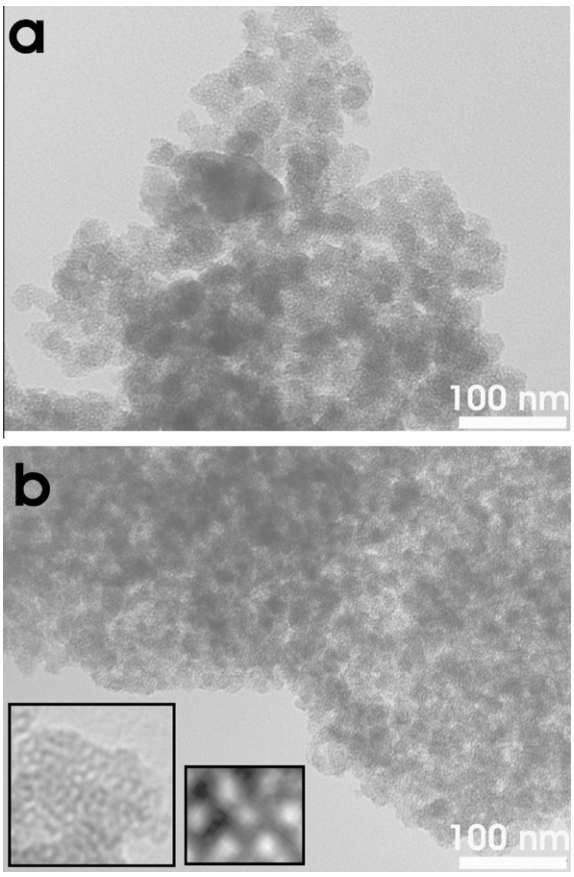

Fig. 7. Representative TEM image of the ScTf-UVM-7 materials. (a) ScOTf-UVM(9), and (b) ScOTf-UVM(50) (with enlarged images 5× and 15× in the insets).

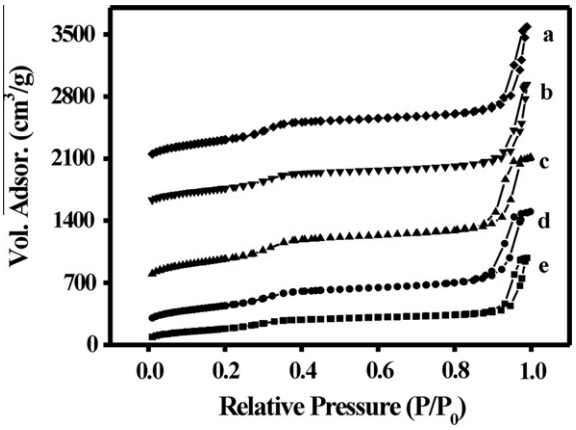

Fig. 8. N_2 adsorption–desorption isotherms of (a) ScOTf-UVM(9), (b) ScOTf-UVM(14), (c) ScOTf-UVM(50), (d) ScOTf-UVM(77), and (e) ScOTf-UVM(250).

changes in the BJH pore sizes occurs with values around 2.6–2.7 nm and 30–50 nm regardless the Sc content for the intra and inter-particle pores, respectively. This data indicate that, even after the incorporation of triflate ligands, no pore blocking occurs. Therefore, the final catalysts maintain a high accessibility to the Sc sites.

In conclusion, the triflic acid plays a double role: (i) as forming agent of triflate complexes with the Sc atoms at the surface and (ii) as solvent for Sc_2O_3 domains by combining an acid attack with the formation of 1:3 triflate complexes ($Sc(OTf)_3$). This last complex is soluble in hydro-alcoholic media, and for this reason, all catalysts have been gently washed with methanol in order to favor its evolution of the mesostructure. A leaching of Sc in this way of *ca.* 30–40% has been estimated (Table 2). The included Sc atoms can be distributed among Sc triflate complexes, Sc sites embedded inside the silica walls and Sc_2O_3 nanodomains (Table 2). Apparently, the proportion of triflate groups is very low and follows an *a priori* unexpected tendency contrary to the Sc amount. In fact, the maximum triflate/Sc molar ratio corresponds to 0.9, and progressively decreases with the Sc content up to values around 0.23. At this point, it is necessary to consider that (1) only a certain proportion of Sc sites are located at the surface (accessible sites for triflate ligands) and (2) the presence of variable amounts of Sc_2O_3 as segregated phase, which in addition are, at least, partially solved in acid triflic acid. Hence, it is evident that the proportion of Sc sites able to form anchored triflate complexes on the silica surface must be clearly diminished.

Samples ScOTf-UVM(9) and ScOTf-UVM(14) are Sc_2O_3 free and have Sc atoms distributed between surface triflate complexes and wall bulk sites. A rough estimation of the proportion of accessible/inaccessible Sc sites can be made from the mesopore wall thickness and the ionic radius of Sc(III). The obtained value (e.g., 68%) is relatively high when compared to related materials containing Al centers. This is due to the relatively thin pore walls (ca. 1.7–1.8 nm regardless the Sc content and *ca.* 2.3–2.6 nm for the Al-related materials) and the large Sc ionic radius. Assuming that only these last Sc atoms can interact with triflate ligands, a corrected S/Sc ratio results, and a more realistic picture of the catalysts can be obtained. Using this correction, it results scandium can coordinate one or two triflate ligands. The 1:1 complex (Sc(OTf)) seems to be the predominant species in all the synthesized catalysts, although a certain content of 1:2 complexes cannot

Table 2
Types and proportion of Sc sites in the ScTf-UVM-7 porous catalysts.

ScTf-UVM-7	Sc/Si[a]	Sc leaching		Sc-OTf ~ (1:1)		S/Sc[d]	$Sc-SiO_2$		Sc_2O_3	
		/Sc/Si[b]	/%	/Sc/Si[c]	/%		/Sc/Si[e]	/%	/Sc/Si[f]	/%
ScOTf-UVM(9)	0.009	0.004	44	0.0034	68	1.3	0.0016	32	~0	~0
ScOTf-UVM(14)	0.014	0.004	29	0.0068	68	1.2	0.0032	32	~0	~0
ScOTf-UVM(50)	0.050	0.013	26	0.0122	33	1.1	0.0058	16	0.019	51
ScOTf-UVM(77)	0.077	0.022	29	0.0163	36	1.0	0.0077	17	0.026	47
ScOTf-UVM(250)	0.250	0.080	32	0.0272	19	1.1	0.0128	9	0.120	72

[a] Sc/Si molar ratio (determined by EPMA) in the Sc-UVM-7 materials before treatment with triflic acid.
[b] Sc leaching during the treatment with triflic acid (determined by EPMA on samples after and before treatment with triflic acid).
[c] Sc/Si molar ratio and % corresponding to complexes Sc:Trifalte ~ 1:1 (estimated value from EPMA, the wall thickness and the size of the Sc(II) specie).
[d] Re-calculated S/Sc molar ratio.
[e] Sc/Si molar ratio and % corresponding to non-coordinated isolated Sc sites (values obtained by difference respect to the total Sc amount measured by EPMA).
[f] Sc/Si molar ratio and % corresponding to Sc_2O_3 domains (determined by XRD).

be discarded. The proportion of Sc_2O_3 has been determined through XRD.

The existence of different Sc species was also confirmed by ^{45}Sc NMR static spectra (Fig. 9). The Sc_2O_3 sample shows a typical complex spectrum with, at least, five well-resolved peaks. This spectrum results from the superposition of the signals associated with two non-equivalent ScO_6 octahedral sites [26].

The Sc-UVM(50) sample displays a similar NMR spectrum, with five principal bands at similar chemical shifts values. This is an expected fact as the ca. the 64% of the Sc in Sc-UVM(50) sample is present in the form of Sc_2O_3 nanodomians. The remaining proportion (36%) of Sc, incorporated inside the mesopore walls or located at the pore surface, must be considered as modifier species of the silica network. In fact, the largest ionic radius of Sc^{3+} (74.5 pm) when compared to Si^{4+} (26 pm) excludes the incorporation of scandium in tetrahedral environments. Probably, a large variety of environments occurs for the remaining isolated scandium atoms ranging from 6 to 8 coordination numbers and different distortion degrees. This multiplicity of possible Sc environments leads to low intensity contributions to the NMR spectrum with subsequent prevalence of a Sc_2O_3-like spectrum. Finally, after treatment with triflic acid, the resulting NMR spectrum preserves some bands that could be attributed to octahedral Sc sites of remaining Sc_2O_3 nanodomains or Sc atoms incorporated as modifiers heteroelements inside the silica framework. Moreover, an intense peak appears at low field that could be tentatively associated with Sc atoms connected to triflate ligands able to remove electron density from the scandium sites. Although an unambiguously signal assignation results very complicated, the evolution of the NMR spectra supports a tendency from rich to low Sc_2O_3 nanodomain proportion due to the attack with triflic acid.

NH_3-DRIFT spectra indicated the presence of Lewis acid sites as inferred from the band located at 1627 cm^{-1}. A band with a smaller intensity located at 1490 cm^{-1} was also detected and assigned to Brønsted acid sites. The relative intensity of Lewis/ Brønsted band ratios indicated a very high excess of the Lewis acid sites (higher than 10). Fig. 10 depicts the evolution of the intensity of these bands for the ScOTf-UVM(9) catalyst with temperature in the range from room temperature to 150 °C. At 150 °C, there are almost only Lewis acid sites.

The spectra recorded for the other catalysts indicated the same bands that were located at the same positions. This fact demonstrate that only one species from those identified from ^{45}Sc NMR spectra exhibits acidity, and by comparison with the spectra collected for pure scandium triflate, these bands should be assigned to incorporated triflates. However, normalized at the same mass of catalyst and at the intensity of the bands measured for ScOTf-UVM(9), the population of the Lewis acid sites in the other catalysts appears to be inferior.

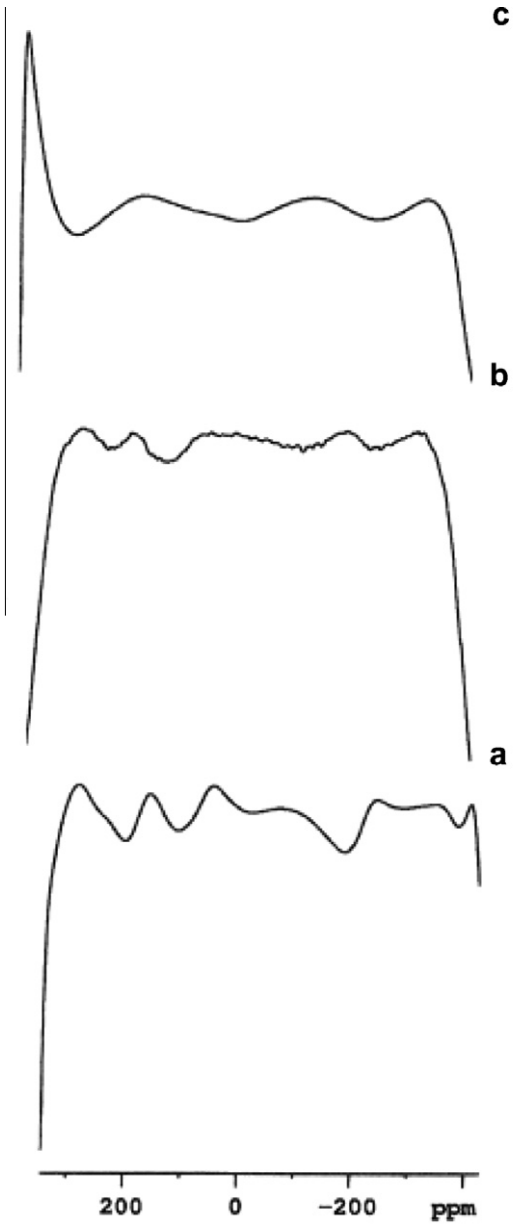

Fig. 9. Static ^{45}Sc NMR spectra of (a) Sc_2O_3, (b) Sc-UVM(50), and (c) ScOTf-UVM(50).

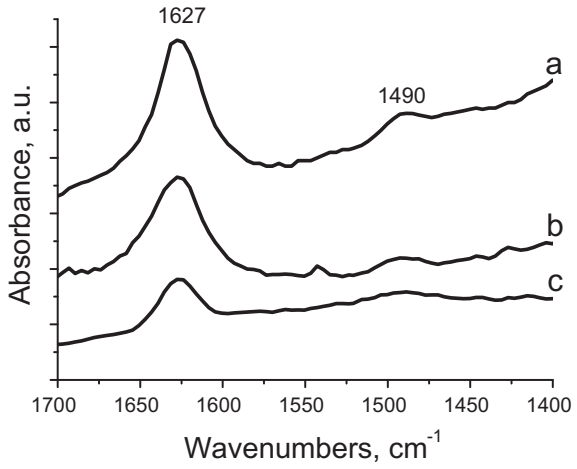

Fig. 10. NH_3-DRIFT spectra of ScOTf-UVM(9) catalyst: (a) room temperature, (b) 50 °C, and (c) 150 °C.

3.2. Catalytic tests

Table 3 compiles the catalytic results using various solvents. These data confirm that N and C alkylation (*ortho-/para*) takes place *via* the reaction of aniline and 4-aminobenzylalcohol (Scheme 1 and Table 3). As a function of the acidity type (Lewis or Brønsted), only 4,4′- and/or 2,4′-MDA primary amines isomers (C alkylation products) were formed as GC chromatography and ^{1}H NMR spectroscopy demonstrated (Fig. 10).

In agreement with Corma et al. [4], different compounds can be well quantified using ^{1}H NMR spectroscopy (Fig. 11): i.e., primary amines (^{1}H NMR δ: 3.7, s, 2H, Ph-C*H2*-Ph), and secondary amines (^{1}H NMR δ: 4.2, s, 2H, Ph-NH-C*H2*-Ph).

Beside C-alkylated isomer, different amounts of a N-alkylated product (Scheme 1, product (3)) were also obtained as a function of both the solvent polarity and the catalyst nature. The highest selectivity to 4,4′-MDA (85.7%) was obtained in acetonitrile (i.e., high dielectric constant, ε) for a conversion of aniline of 31.4%. Such a behavior may suggest the reaction takes place through highly polar intermediates. Significant changes in conversion rate, *ortho/para* isomer ratio and amount of N-alkylated species occur depending on the Sc/Si molar ratio (Table 3).

The observed tendencies are not correlated with the Sc content, because different Sc sites are formed but only one exhibits strong Lewis acidity (Table 2). Thus, competition phenomena and even poisoning effects can be expected. Hence, the concentration, nature, and distribution of the different Sc species must be analyzed and correlate in order to understand the catalytic results.

The correlation of the catalysts nature with their behavior in the synthesis of 4,4′-MDA revealed that the process requires indeed not only a high polar environment but also strong acid Lewis sites (Sc triflate complexes in our case) as active sites. Accordingly, ScOTf-UVM(9) and ScOTf-UVM(14) catalysts show high aniline conversion and selectivity toward the desired 4,4′-MDA product. On the other hand, the detection of N-alkylated species unambiguously supports the two-step mechanism when Lewis acids are present. The key role played by Lewis acid sites is sustained by the catalytic tests with $Sc(OTf)_3$ (99%, Aldrich, a very strong Lewis acid) (Table 3). The fact that the ScOTf-UVM(9) sample displays catalytic performances closer to the commercial $Sc(OTf)_3$ indicates that the highly dispersed Sc triflate species behave as very strong Lewis acids able to rearrange the N-alkylated intermediate in 4,4′-MDA isomer. Nevertheless, in the presence of Nafion-embedded silica sample (SAC-13 Aldrich, a superacidic Brønsted acidic material), the main product is 2,4′-MDA (95.4%) for a conversion of 27.0% (Table 3). Thus, dealing with the *ortho/para* isomer ratio, the nature of the acid sites (Lewis or Brønsted) constitutes an additional key parameter. Moreover, the selection of the UVM-7-like highly accessible support architecture allows us to minimize the diffusion and steric constraints present in zeolites.

Fig. 12 depicts the variation of TON as a function of the normalized intensity of the Lewis band. This variation clearly demonstrates the direct relation between the catalysts activity and the Lewis acid sites concentration.

Abrupt changes both in conversion and selectivity were observed with the Sc/Si ratio. As the Sc content increases, the number of Brønsted acid sites is expected to increase due to the Sc_2O_3 nanoparticle surface or Sc_2O_3–silica interface and the Sc(III) atoms embedded on the silica walls. These sites could be responsible for

Table 3
The catalytic performances as a function of the reaction parameters and the catalyst (Sc/Si ratio) nature.

Catalyst	Solvent (ε)	$X_{aniline}$ (%)	TON	$S_{C\text{-}alkylates}$ (%)	$S_{isomers}$ (%) $S_{2,4'\text{-}MDA}$ (%)	$S_{4,4'\text{-}MDA}$ (%)
UVM-7	Acetonitrile (37.0)	0	0	–	–	–
ScOTf-UVM(9)	Hexan (2.0)	4.9	28.0	20.8	0	>99.9
	THF (7.5)	8.8	50.4	39.9	0	>99.9
	Ethanol (30.0)	13.9	79.4	49.6	0	>99.9
	Acetonitrile (37.0)	31.4	180	85.7	0	>99.9
	Acetonitrile (37.0)[a]	40.2	230	88.9	0	>99.9
	Acetonitrile (37.0)[b]	39.6	226	90.9	0	>99.9
ScOTf-UVM(14)	Acetonitrile	32.0	91.2	74.2	0	>99.9
ScOTf-UVM(50)	Hexan	1.6	2.6	99.9	89.6	10.4
	THF	3.3	5.4	99.1	75.6	24.4
	Ethanol	7.4	12.1	99.9	73.8	26.2
	Acetonitrile	12.3	20.2	100	79.2	20.8
ScOTf-UVM(77)	Acetonitrile	10.0	12.3	99.9	77.8	22.2
ScOTf-UVM(250)	Acetonitrile	2.1	1.5	99.8	80.0	20.0
$Sc(OTf)_3$[c]	Acetonitrile	33.1	10.8	95.5	0	>99.9
SAC-13[d]	Acetonitrile	27.0	120	95.4	>99.9	0

Reaction conditions: aniline/4-aminobenzylalcohol molar ratio = 2/1; 2 mmol (0.186 g) of aniline; 1 mmol (0.123 g) of 4-aminobenzylalcohol; 30 mg of catalyst; 3 mL of solvent; temperature = 80 °C, reaction time = 24 h.

[a] Temperature = 140 °C.

[b] Microvawes conditions: aniline/4-aminobenzylalcohol molar ratio = 2/1; 6 mmol (0.558 g) of aniline; 3 mmol (0.369 g) of 4-aminobenzylalcohol; 90 mg of catalyst; 12 mL of solvent; temperature = 80 °C, reaction time = 3 h.

[c] Commercial $Sc(OTf)_3$ (99%, Aldrich).

[d] Commercial SAC-13 (Nafion-embedded silica, 13 wt.%, Aldrich).

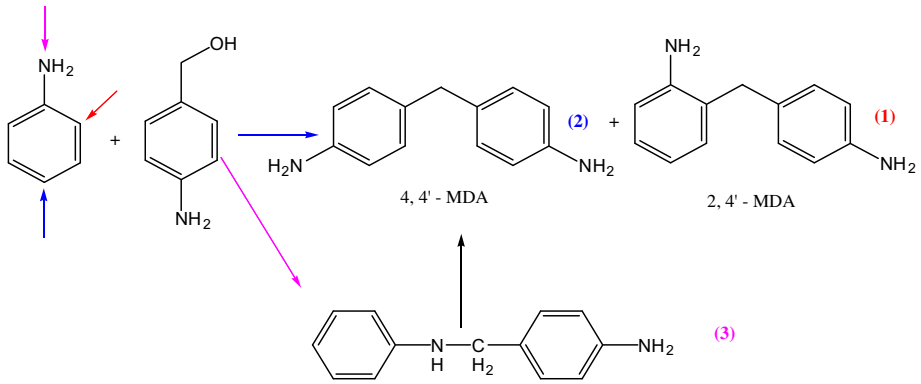

Scheme 1. The synthesis of 4,4′-MDA by condensation of aniline with 4-aminobenzylalcohol.

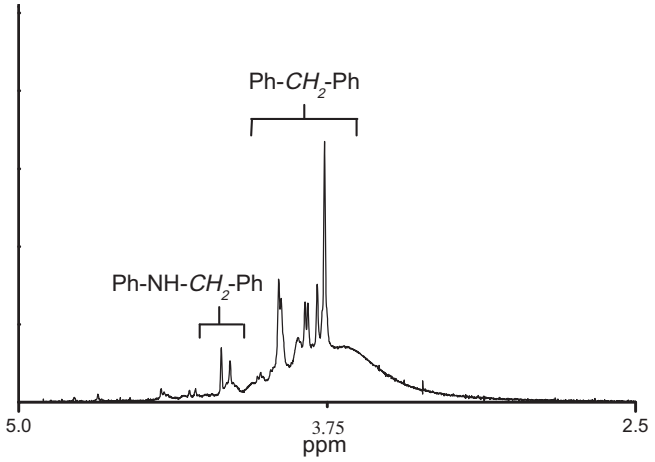

Fig. 11. ^{1}H NMR characterization of a reaction sample showing the different groups of products determined.

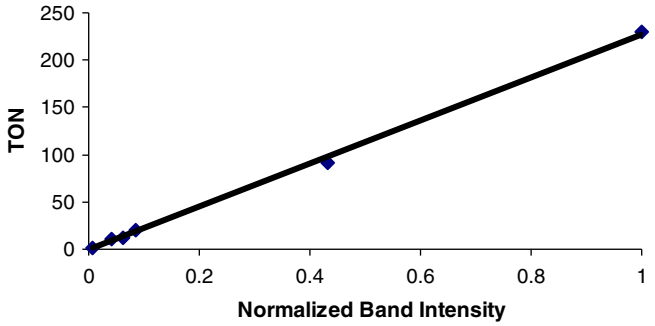

Fig. 12. The variation of TON as a function of the normalized intensity of the Lewis band.

the observed inversion in the ortho/para isomer ratio. Finally, regardless the proportion of Lewis and/or Brønsted acid sites, the presence of Sc_2O_3 domains (even at low amounts) seems to induce a poisoning effect as the conversion values decrease up to ca. 2%.

According to Hart and Kosak [27], the presence of a Lewis acid catalyst induces a Reilly–Hickinbottom rearrangement of N-benzylaniline intermediates with the formation of the *para* isomer (e.g., 4,4′-MDA in the studied synthesis), while the presence of a typical Brønsted acid catalyst favors the alkylation of aniline with the formation of the *ortho*-C-alkylated isomer. Schemes 2 and 3 describe this mechanism. As expected, the use of these new catalysts led to a higher proportion of N-alkylates compared to values achieved on $Sc(OTf)_3$. This can be easily interpreted in terms of a necessary steric hindrance to achieve the rearrangement that can be provided by the heterogeneous catalyst inside the mesopores.

With the wish of optimization, both the conversion of aniline and the selectivity to 4,4′-MDA, a series of catalytic tests in the presence of ScOTf-UVM(9), were carried out varying the reaction parameters. The increase of the reaction temperature from 80 °C to 140 °C has only a small influence upon the catalytic performances: at 140 °C, the conversion reached 40.2% (Table 3, entry 6, compared with 31.4%, at 80 °C, Table 3, entry 5) while the selectivity to 4,4′-MDA reached 88.9% (Table 3, entry 6, compared with 85.7%, at 80 °C, Table 3, entry 5) after 24 h. Interestingly, by using microwaves, the same selectivity level (90%) was reached in only 3 h (Table 3, entry 7). As expected, the increase of the catalyst amount led to increased conversions.

On the other hand, the catalytic tests using a stoichiometric aniline/4-aminobenzylalcohol molar ratio of 1/1 led to a conversion of aniline and a selectivity to 4,4′-MDA lower than 5%, at 80 °C after 24 h.

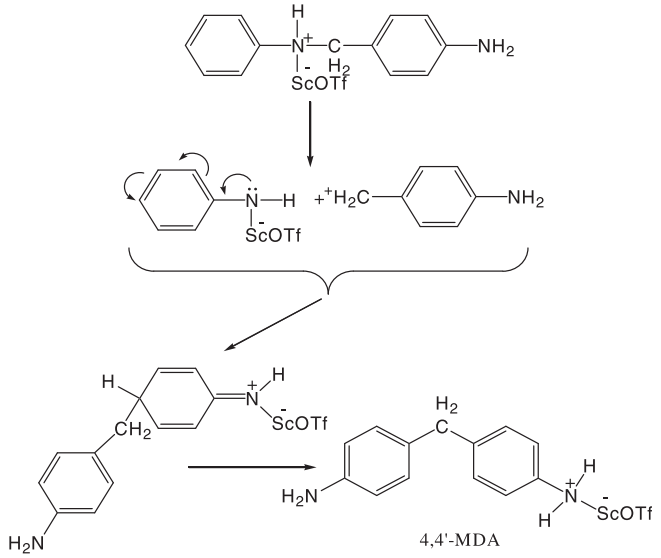

Scheme 2. The Reilly–Hickinbottom rearrangement of the N-alkylated intermediate to 4,4′-MDA.

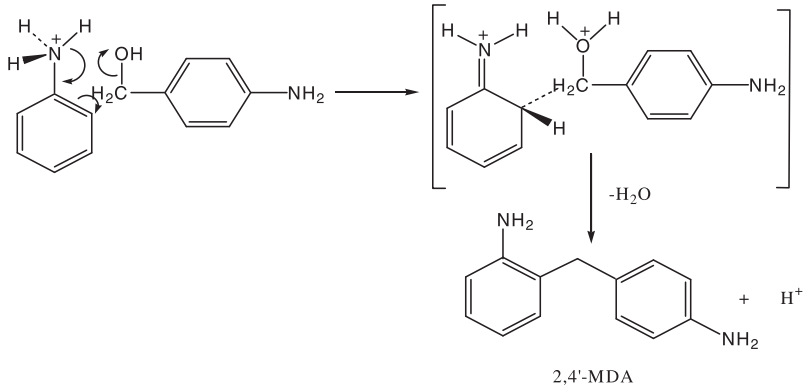

Scheme 3. The alkylation of aniline with 4-aminobenzylic alcohol in the presence of Brønsted species with the formation of 2,4′-MDA.

Table 4
Recycling of ScOTf-UVM(9) in four catalytic runs.

Crt. Nr.	Run	$X_{aniline}$ (%)	$S_{C\text{-}alkylated}$ (%)	$S_{isomers}$ (%)	
				$S_{2,4'\text{-}MDA}$ (%)	$S_{4,4'\text{-}MDA}$(%)
1	Fresh catalyst (1st run)	31.4	85.7	0	>99.9
2	2nd run	31.2	85.1	0	>99.9
3	3rd run	31.3	85.4	0	>99.9
4	4th run	31.3	85.5	0	>99.9

Reaction conditions: aniline/4-aminobenzylalcohol molar ratio = 2/1; 2 mmol (0.186 g) of aniline; 1 mmol (0.123 g) of 4-aminobenzylalcohol; 30 mg of catalyst; 3 mL of acetonitrile solvent (AcCN); temperature = 80 °C; reaction time = 24 h.

Recycling these catalysts (ScOTf-UVM) for five times in the above reactions was not accompanied by any visible loss of conversion and selectivity (Table 4).

Besides, the chemical analysis of the reaction products clearly indicated no leaching of the triflate ligands from around scandium sites. As another research groups demonstrated [28,29] such an evolution from Sc triflates to triflic acid, under reaction conditions, should be observed in a change in the regioselectivity in a second use of the catalyst. In this case, the lack of region-isomers from the second catalytic charge (see Table 4) can be an indication of the scandium triflate sites stability during the catalytic reaction.

4. Conclusion

To summarize, the novel mesoporous ScOTf-UVM-7 materials has been found to be effective catalysts for the synthesis of 4,4′-MDA from aniline and 4-aminobenzylalcohol, as a function of the scandium content and the nature of the formed Sc species. Conversions of around 30% with a selectivity to 4,4′-MDA higher than 85% can be obtained in moderate reaction conditions: 80 °C, aniline/4-aminobenzyl alcohol molar ratio of 2/1, aniline/Sc-OTf active sites ratios of over 550 (2 mmol of aniline for 0.0034 mmol of Sc-OTf (1:1) species in ScOTf-UVM(9) sample), after 24 h. Similar catalytic performances can be obtained in only 3 h using a microwaves-assisted condensation reaction. Similar conversions were obtained on ScOTf-UVM(14) sample but the selectivity to 4,4′-MDA decreased in *ca.* 10%. The catalysts can be several times recycled without a significant loss of the catalytic performances. A reason of this high stability is the recognized behavior of scandium triflate toward highly polar solvents comparing to other Lewis acids. On the other side, the advantage of using solid catalysts instead of homogeneous ones (e.g., HCl) is the elimination of the additional steps for neutralization and separation of the reaction products. Moreover, by using 4-aminobenzylalcohol instead of formaldehyde, the synthesis may be substantially improved in terms of productivity and simplicity, avoiding the formation of many by-products.

Acknowledgment

Prof. Vasile I. Parvulescu thanks UEFISCDI for the financial support (project 275/5.10.2011).

References

[1] A. de Angelis, P. Ingallina, C. Perego, Ind. Eng. Chem. Res. 43 (2004) 1169.
[2] J.L. Nafzinger, L.A. Rader, I.J. Seward, U.S. Patent, 4554,378, 1985, to The Dow Chemical Company.
[3] F.F. Frulla, A.A.R. Sayigh, H. Ulrich, P.J. Whitman, U.S. Patent, 4039,580, 1977, to The Upjohn Company.
[4] A. Corma, P. Botella, C. Mitchell, Chem. Commun. (2004) 2008.
[5] T. Kugita, S. Hirose, S. Namba, Catal. Today 111 (2006) 275.
[6] Y. Kiso, T. Takai, T. Hayashi, Eur. Patent, 0329,367.
[7] M. Salzinger, M.B. Fichtl, J.A. Lercher, Appl. Catal. A: Gen. 393 (2011) 189.
[8] M. Salzinger, J.A. Lercher, Green Chem. 13 (2011) 149.
[9] E. Reale, A. Leyva, A. Corma, C. Martinez, H. Garcia, F. Rey, J. Mater. Chem. 15 (2005) 1742.
[10] S.M. Coman, G. Pop, C. Stere, V.I. Parvulescu, J. El Haskouri, D. Beltran, P. Amoros, J. Catal. 251 (2007) 388.
[11] N. Candu, S.M. Coman, V.I. Parvulescu, J. El Haskouri, P. Amoros, D. Beltran, Appl. Catal. A: Gen. 372 (2010) 58.
[12] N. Candu, M. Musteata, S.M. Coman, V.I. Parvulescu, J. El Haskouri, P. Amoros, D. Beltran, Chem. Eng. J. 161 (2010) 363.
[13] Cl.T. Brinden, C.D. Williams, D. Apperley, Inorg. Mater. 43 (2007) 758.
[14] K. Mantri, K. Komura, Y. Kubota, Y. Sugi, J. Mol. Catal. A: Chem. 236 (2005) 168.
[15] S. Kobayashi, I. Hachiya, M. Araki, H. Ishitani, Tetrahedron Lett. 34 (1993) 3755.
[16] J. El Haskouri, D. Ortiz de Zarate, C. Guillem, J. Latorre, M. Caldes, A. Beltrán, D. Beltrán, A.B. Descalzo, G. Rodríguez, R. Martínez-Mañez, M.D. Marcos, P. Amorós, Chem. Commun. (2002) 330.
[17] L. Huerta, C. Guillem, J. Latorre, A. Beltrán, R. Martínez-Mañez, M.D. Marcos, D. Beltrán, P. Amorós, Solid State Sci. 8 (2006) 940.
[18] J. El Haskouri, J.M. Morales, D. Ortiz de Zárate, L. Fernández, J. Latorre, C. Guillem, A. Beltrán, D. Beltrán, P. Amorós, Inorg. Chem. 47 (2008) 8267.
[19] C.F. Baes, R.E. Mesmer, The Hydrolysis of Cations, John Wiley & Sons, New York, 1976.
[20] W.W. Rudolph, C.C. Pye, J. Solution Chem. 29 (2000) 955.
[21] P. Lindqvist-Reis, I. Persson, M. Sandström, Dalton Trans. (2006) 3868.
[22] J.G. Verkade, Acc. Chem. Res. 26 (1993) 483.
[23] J. Pinkas, J.G. Verkade, Polyhedron 15 (1996) 1567.
[24] A.A. Naiini, V. Young, J.G. Verkade, Polyhedron 14 (1995) 393.
[25] P. Kansal, R.M. Laine, J. Am. Ceram. Soc. 80 (1997) 2597.
[26] D. Khabibulin, K. Romanenko, M. Zuev, O. Lapina, Magn. Reson. Chem. 45 (2008) 962.
[27] H. Hart, J.R. Kosak, J. Org. Chem. 27 (1962) 116.
[28] J.R. Cabrero-Antonino, A. Leyva-Pérez, A. Corma, Adv. Synth. Catal. 352 (2010) 1571.
[29] L. Coulombel, F. Grau, M. Weïwer, I. Favier, X. Chaminade, A. Heumann, J. Carles Bayón, P.A. Aguirre, E. Duñach, Chem. Biodifversity 5 (2008) 1070.